IEEE Journal on Exploratory Solid-State Computational Devices and Circuits

Received 10 September 2019; revised 13 October 2019; accepted 2 November 2019.
Date of publication 6 November 2019; date of current version 6 February 2020.

Digital Object Identifier 10.1109/JXCDC.2019.2951767

Toggle Spin-Orbit Torque MRAM With Perpendicular Magnetic Anisotropy

NAIMUL HASSAN[1] (Student Member, IEEE), SUSANA P. LAINEZ-GARCIA[1], FELIPE GARCIA-SANCHEZ[2,3] (Member, IEEE), and JOSEPH S. FRIEDMAN[1] (Senior Member, IEEE)

[1]Electrical & Computer Engineering, The University of Texas at Dallas, Richardson, TX 75080 USA
[2]Departamento de Física Aplicada, Universidad de Salamanca, 37008 Salamanca, Spain
[3]Instituto Nazionale di Ricerca Metrologica, 10135 Turin, Italy

CORRESPONDING AUTHOR: J. S. FRIEDMAN (joseph.friedman@utdallas.edu)

ABSTRACT Spin-orbit torque (SOT) is a promising switching mechanism for magnetic random-access memory (MRAM) as a result of the potential for improved switching speed and energy efficiency. It is of particular interest to develop an SOT-MRAM device with perpendicular magnetic anisotropy (PMA) in order to leverage the greater density and thermal stability achievable with PMA as opposed to in-plane magnetic anisotropy. However, the orthogonality between SOT and PMA prevents deterministic directional switching without an additional device component that breaks the symmetry, such as an external magnetic field or complex physical structure; not only do these components complicate fabrication, they also are not robust to variations in fabrication and applied switching current. Following previous work demonstrating toggle SOT switching of ferromagnetic layers, this article, therefore, proposes a simple SOT-MRAM structure with PMA in which deterministic toggle switching is achieved without requiring additional device components. Furthermore, this toggle PMA SOT-MRAM is shown to be far more robust than previous approaches for directional PMA SOT-MRAM, with no maximum current pulse duration and greater than 50% tolerance to applied switching current magnitude. This article describes the physical structure and toggle switching mechanism, provides micromagnetic simulations demonstrating its feasibility, and evaluates the robustness and tolerance to material parameters to guide the fabrication of optimized devices that will jumpstart the third generation of MRAM.

INDEX TERMS Magnetic random-access memory (MRAM), perpendicular magnetic anisotropy (PMA), spin-orbit torque (SOT), toggle switching.

I. INTRODUCTION

MAGNETIC random-access memory (MRAM) is a promising candidate for next-generation data storage due to its nonvolatility [1], high speed, and energy efficiency [1]–[3]. The core of each MRAM bit cell is composed of a magnetic tunnel junction (MTJ) that can be switched between two resistance states, and this MTJ is accompanied by complementary circuitry to read and write the magnetic state. Following the development of MRAM switching driven by a magnetic field, spin-transfer torque (STT)-MRAM has become preeminent due to its increased density and energy efficiency. In particular, STT-MRAM with perpendicular magnetic anisotropy (PMA) is preferred over in-plane anisotropy due to its higher density [4] and increased thermal stability, which results in a longer data retention time. However, STT-MRAM has several limitations resulting from sharing the read and write path, including degradation of the tunnel barrier from repeated switching. Therefore, spin-orbit torque (SOT) switching has recently been developed in order to overcome the limitations of STT by decoupling the write current path from the MTJ tunnel barrier.

However, SOT produces a spin current polarized in the in-plane direction, which cannot switch an MTJ with PMA. Several approaches have recently been developed to break the SOT symmetry, thereby enabling SOT-MRAM with PMA: one approach is to apply an in-plane magnetic field along the direction of the writing current [5], [6]; another approach involves the deformation of the structure [7], [8]; a third

This work is licensed under a Creative Commons Attribution 4.0 License. For more information, see http://creativecommons.org/licenses/by/4.0/

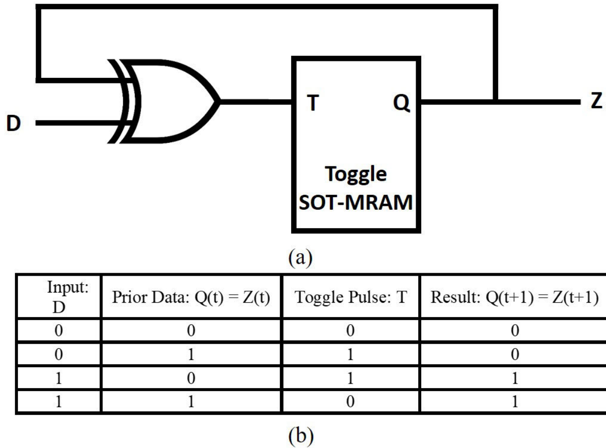

Input: D	Prior Data: Q(t) = Z(t)	Toggle Pulse: T	Result: Q(t+1) = Z(t+1)
0	0	0	0
0	1	1	0
1	0	1	1
1	1	0	1

FIGURE 1. (a) Circuit and (b) logical relationship to perform directional switching with a toggle memory device. By comparing the input bit (*D*) with the prior data (*Q*) and writing the output into the SOT-MRAM, the toggle mechanism can be converted to directional switching. The purpose of this circuit is to apply a toggle pulse (*T*) to the SOT-MRAM only when the incoming bit is different from the stored bit, thus resulting in directional memory storage with a simple XOR operation. When $D \neq Q$, the toggle pulse becomes logical 1 and results in the inversion of the memory state *Z*; when $D = Q$, there is no toggle pulse, and *Z* retains its prior state.

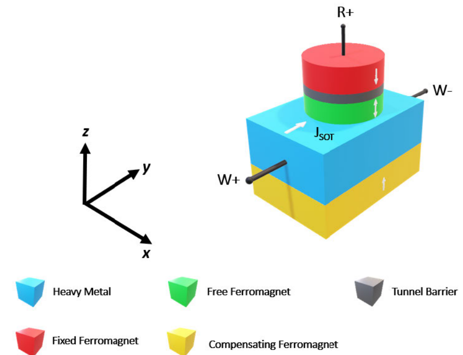

FIGURE 2. Schematic of the three-terminal MTJ for toggle MRAM, with state recorded in the free layer and a compensating ferromagnet for stray field cancellation. Write current from W+ to W− creates SOT that switches the magnetization of the free ferromagnet; the state of the MTJ can be read by applying a voltage between R+ and W−.

requires tilting of the anisotropy by wedge-shaped ferromagnets [4]; another uses an antiferromagnet–ferromagnet bilayer system [9]; a fifth uses competing spin currents [10]; another requires five terminals [11]; and a seventh needs an SOT current of a precise magnitude [12]. Unfortunately, all of these approaches increase the fabrication complexity, are highly sensitive to the switching current duration and magnitude, or increase the switching energy. It is, therefore, critical to develop an energy-efficient PMA SOT-MRAM that is simple to fabricate, robust to switching current parameters, and does not require an external magnetic field.

Leveraging the SOT toggle switching suggested by Legrand *et al.* [13], we therefore propose toggle PMA SOT-MRAM that exploits the precessional nature of field-like SOT to achieve field-free and energy-efficient switching with a simple structure that is robust to the switching current magnitude and duration. We apply unidirectional SOT current pulses that toggle the PMA MRAM between the parallel and antiparallel states. With this toggle switching, each SOT pulse flips the stored magnetization irrespective of its initial direction; the write circuit can use this toggle switching mechanism for selective directional switching [14], [15]. This toggle switching is in contrast to the bidirectional currents required for conventional SOT-MRAM devices with directional switching, and is analogous to Savtchenko toggle switching of commercially available field-switched MRAM [16]. (See Fig. 1 for the circuit and logical relationship to perform directional switching with a toggle memory device.) This toggle SOT-MRAM device is highly robust to the switching current magnitude and duration, thus simplifying the write circuit and improving system efficiency. In particular, this switching phenomenon is shown here to tolerate write current imprecision greater than 50% and rise times slower than 200 ps, and has no maximum write current duration. Furthermore, the device structure consists of a minimal number of planar layers, thereby simplifying fabrication and increasing the potential for continued MRAM scaling. The proposed memory device thus provides the first robust approach to simultaneously leverage the energy efficiency of SOT and the thermal stability of PMA without requiring complex fabrication or an external magnetic field.

II. TOGGLE SOT-MRAM DEVICE

The structure of the SOT-driven toggle PMA MRAM is shown in Fig. 2 as a three-terminal MTJ [17] composed of a compensating ferromagnet, heavy metal, free ferromagnet, insulating tunnel barrier, and fixed ferromagnet. Current through the heavy metal induces SOT on the adjacent free ferromagnet, while the compensating ferromagnet cancels the stray field. Both the free and fixed ferromagnets have PMA, with a $\hat{z}$-directed easy axis and a hard x-y plane. The magnetization of the fixed ferromagnet is in the $-\hat{z}$-direction through an antiferromagnetic coupling, while the free ferromagnet can toggle between stable relaxed states in the $+\hat{z}$- and $-\hat{z}$-directions by applying a unidirectional current of a certain range through the write path. The resistance state of the MTJ can be determined through the tunneling magnetoresistance effect with a small current passed through the read path.

This magnetization switching mechanism can be understood as follows for an initial low magnetoresistance state where both ferromagnet magnetizations are stable in the $-\hat{z}$-direction [see Fig. 3(a)]. When a write current is applied through the heavy metal in the $+\hat{y}$-direction, a $+\hat{z}$-directed SOT spin current is produced and is polarized in the $-\hat{x}$-direction. The interplay between the PMA field ($\mu_0 H_K \hat{z}$) and the field-like (H_T) and damping-like (H_L) components of the SOT causes the magnetization $\hat{m}$ of the free ferromagnet

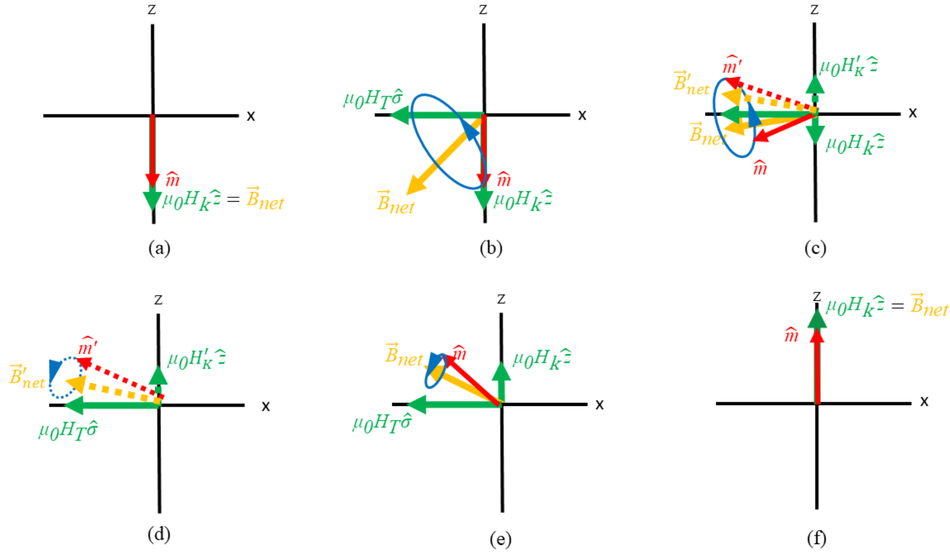

FIGURE 3. **Toggle switching process. (a) Free layer magnetization $\hat{m}$ is initially relaxed at $-\hat{z}$-direction before the application of SOT excitation. (b) Application of field-like SOT, $\mu_0 H_T \hat{\sigma}$, causes $\hat{m}$ to precess around $\vec{B}_{\text{net}}$. (c) Gilbert damping decreases the radius of the circular trajectory and applies a torque on $\hat{m}$ to align it along $\vec{B}_{\text{net}}$. Meanwhile, the magnitude and direction of $\vec{B}_{\text{net}}$ also changes due to the varying PMA field $\mu_0 H_{K,\text{eff}} m_z \hat{z} = \mu_0 H_K \hat{z}$. (d) The precessional and damping forces cause both $\hat{m}$ and $\vec{B}_{\text{net}}$ to cross the hard *x-y* plane as the radius of the circular trajectory continues to decrease. (e) The radius of the circular trajectory approaches zero with $\hat{m}$ and $\vec{B}_{\text{net}}$ across the hard *x-y* plane, causing $\hat{m}$ to reach a stable excited state at an energy minimum. (f) Switching off the SOT excitation causes $\hat{m}$ to relax in the $+\hat{z}$-direction (nearest easy axis direction), opposite the initial state.**

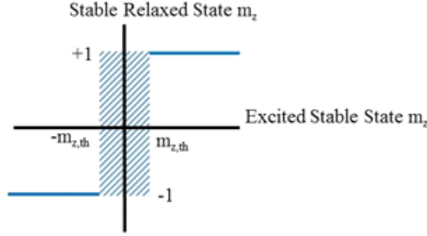

FIGURE 4. **SOT excited stable state versus stable relaxed state. In the graph, the hashed portion between thresholds $+m_{z,\text{th}}$ and $-m_{z,\text{th}}$ is the region where thermal noise may cause unpredictable behavior.**

to precess around the net magnetic field of the system, $\vec{B}_{\text{net}}$ [see Fig. 3(b)]. $\hat{m}$ crosses the hard x-y plane as it precesses [see Fig. 3(c)] and the radius gradually decreases [see Fig. 3(d)], eventually reaching a stable state with positive z magnetization not aligned with the easy axis [see Fig. 3(e)]. Once the SOT current excitation is removed, $\hat{m}$ relaxes to the nearest position along the easy axis in the $+\hat{z}$-direction (see Fig. 4), switching the MTJ to a high magnetoresistance state [see Fig. 3(f)]. When the next write current is applied, the magnetization of the free ferromagnet toggles back to the $-\hat{z}$-direction; as $\hat{m}$ crosses the hard x-y plane exactly once during each application of an SOT current, the MTJ toggles between the parallel and antiparallel states every time an SOT current is applied.

This toggle switching is demonstrated via the micromagnetic simulations [18] of Fig. 5. The circular monodomain free ferromagnet has 30 nm diameter and 1.2 nm thickness, and the material parameters are taken from Zhang *et al.* [19] (see the Appendix). As shown in Fig. 3(a) and (b), the magnetization is initialized at $m_z = -1$, and the application of the SOT current causes $\hat{m}$ to cross the hard axis and reach a stable excited state with $m_z = +0.4$. When the SOT current is removed, $\hat{m}$ precesses around the easy axis as it relaxes to $m_z = +1$, having flipped its orientation relative to the easy axis. Repeated SOT current pulses cause this toggle MRAM to switch magnetization states with each pulse, as demonstrated in Fig. 5(c) with four consecutive SOT pulses of 4 ns duration with 10 ns of relaxation between each.

III. ROBUSTNESS OF DETERMINISTIC SWITCHING MECHANISM

This toggle MRAM device is promising for the next generation of nonvolatile memory due to its simplicity and robustness to input excitation. To demonstrate the exceptional robustness of this toggle MRAM switching, micromagnetic simulations were performed to determine the sensitivity of the switching process on the current amplitude and dynamics. Furthermore, our results provide material design guidelines to maximize the robustness of the switching phenomenon.

To evaluate this robustness—and therefore the precision required to design a CMOS driver circuit—we define the toggle range within which the switching mechanism behaves properly as

$$\text{Toggle Range} = \mu_0 H_{L,\max} - \mu_0 H_{L,\min} \tag{1}$$

where $\mu_0 H_{L,\min}$ and $\mu_0 H_{L,\max}$ denote the maximum and minimum damping-like SOT fields, respectively, for which the toggle switching proceeds properly. As can be seen in Fig. 6(a), damping-like SOT fields smaller than $\mu_0 H_{L,\min}$ are insufficient to cause the free ferromagnet magnetization to cross the hard axis; therefore, no switching

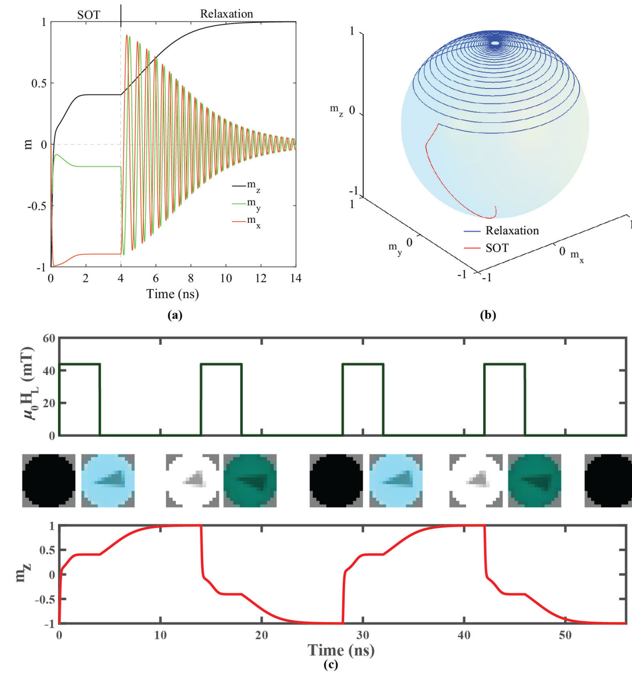

FIGURE 5. Micromagnetic simulation of toggle switching. (a) Time versus normalized magnetization. We inject an SOT current for 4 ns, and then let the system relax in the absence of current. $\hat{m}$ is initially in the $-\hat{z}$-direction, crosses the hard axis at $t = \sim$180 ps, and reaches a stable excited state of $m_z = 0.4$ at $t = \sim$2 ns. After the current is switched off at $t = 4$ ns, $\hat{m}$ relaxes along the $+\hat{z}$-direction. (b) Trajectory of $\hat{m}$ in a unit sphere during SOT excitation (red) and relaxation (blue). (c) Multiple 4-ns SOT currents are applied with magnetic field $\mu_0 H_L$, causing m_z to toggle with each applied SOT current pulse, as depicted via micromagnetic simulation screenshots that demonstrate switching between the $+\hat{z}$-(white) and $-\hat{z}$-(black) directions.

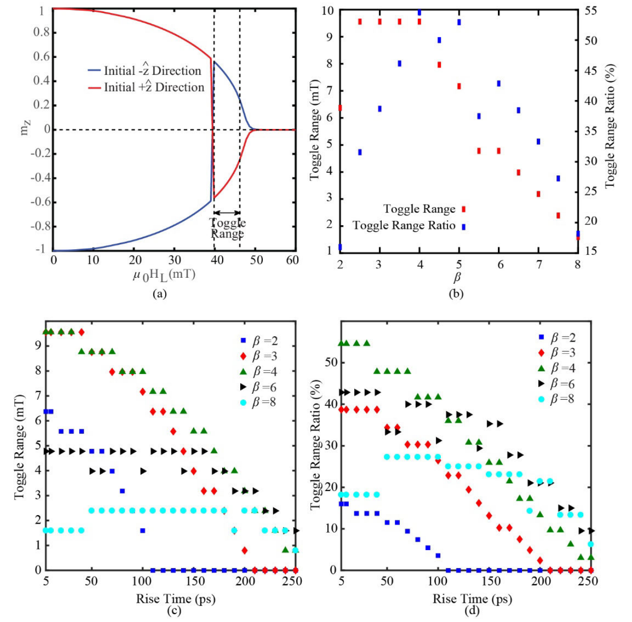

FIGURE 6. Sensitivity of the toggle switching to variations in damping-like SOT field strength, rise time, and β. (a) Stable excited state magnetization as a function of damping-like SOT field $\mu_0 H_L$. The dotted vertical lines denote the boundary of the toggle range for magnetization threshold $|m_{z,\mathrm{th}}| = 0.2$. (b) Toggle range and toggle range ratio as a function of β for a step damping-like SOT excitation (zero rise time). (c) Toggle range as a function of rise time for various β values, illustrating that the damping-like SOT field strength becomes less sensitive to rise time for higher β values. (d) Rise time versus toggle range ratio for various β values.

occurs. For damping-like SOT fields greater than $\mu_0 H_{L,\max}$, the excited stable state is so close to the hard axis that thermal noise can cause $\hat{m}$ to relax in an unpredictable manner, which is highly problematic for memory applications. In particular, we use a threshold of $m_z = |0.2|$ which is stricter than the 0.15 value used by Torrejon *et al.* [20] and ensures relaxation in less than 10 ns. For a robustness metric, more relevant to device and circuit fabrication, we further define the toggle range ratio as

$$\text{Toggle Range Ratio} = \frac{\mu_0 H_{L,\max} - \mu_0 H_{L,\min}}{\mu_0 H_{L,\min}} = \frac{J_{\mathrm{SOT},\max} - J_{\mathrm{SOT},\min}}{J_{\mathrm{SOT},\min}} \quad (2)$$

where $J_{\mathrm{SOT},\min}$ and $J_{\mathrm{SOT},\max}$ denote the actual maximum and minimum in-plane current values through the heavy metal layer corresponding to proper toggle switching.

Based on these metrics, the robustness to the magnitude and rise time of the SOT current pulse is analyzed for various ratios between the transverse magnetic field $\mu_0 H_T \hat{\sigma}$ and longitudinal magnetic field $\mu_0 H_L (\hat{m} \times \hat{\sigma})$, expressed as the field-to-damping component ratio β as a function of the spin polarization direction of SOT current, $\hat{\sigma}$.

β values ranging from 2 to 8 have been reported [21], with Legrand *et al.* [13] having demonstrated toggle switching for β values between 1.82 and 4.35. As shown in Fig. 6(b), the toggle range is maximized in the β range explored by Legrand *et al.* [13], with the toggle range ratio above 50% for β between 4 and 5 for step current pulses with zero rise time. The toggle range and ratio decay with increased rise time as shown in Fig. 6(c) and (d), though proper toggle switching persists for rise times greater than 200 ps. Importantly, it is observed that the toggle range ratio for $\beta = 4$ remains greater than 50% for rise time less than 50 ps; this ratio is significantly larger than that previously demonstrated with directional SOT switching in a deformation free antiferromagnet–ferromagnet bilayer system by an energy-efficient noncompeting current [9]. It should also be noted that while large β values do not provide a particularly large toggle range and ratio in response to step inputs, large β values provide the greatest toggle range and ratio for SOT current pulses with a large rise time. As mentioned previously, this toggle switching mechanism provides the additional advantage of permitting a long current pulse; there is no maximum current pulse duration.

Further analyses have been performed to evaluate the impact of relaxation time and PMA field on this toggle switching mechanism, and to demonstrate its determinism at room temperature. As shown in Fig. 7, a larger anisotropy

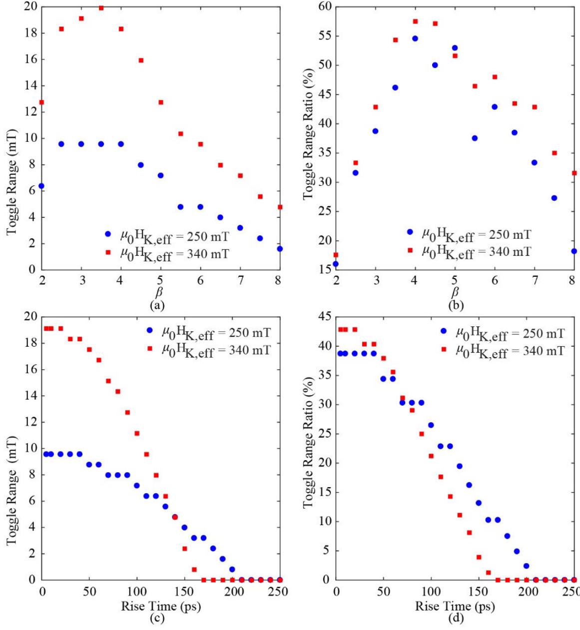

FIGURE 7. Effect of magnetic anisotropy on toggle switching. (a) β versus toggle range. (b) β versus toggle range ratio for step SOT excitation. (c) Rise time versus toggle range for $\beta = 3$. (d) Rise time versus toggle range ratio for $\beta = 3$. As shown in (a) and (b), the higher $\mu_0 H_{K,\text{eff}} = 340$-mT sample provides larger toggle range and toggle range ratio for $t_{\text{rise}} = 0$. However, as shown in (c) and (d), the toggle range decreases at a faster rate with an increasing t_{rise} as compared to the lower anisotropy sample. Beyond $t_{\text{rise}} = 50$ ps for a β value of 3, the lower anisotropy sample performs better from a toggle range ratio perspective.

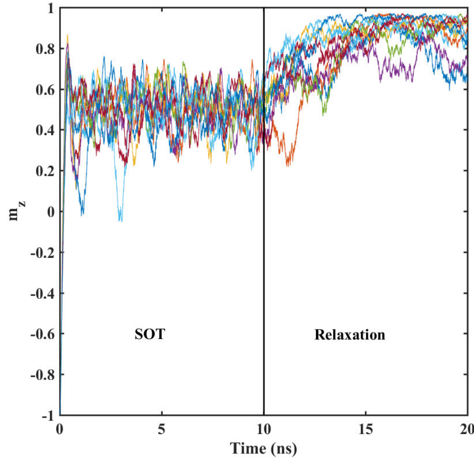

FIGURE 8. Room temperature micromagnetic simulation. The ten different colors represent ten distinct thermal simulation results for 10 ns SOT pulse of $\mu_0 H_L = 17.5$ mT with 20 ps rise time and 10 ns relaxation applied to a free ferromagnet with $\mu_0 H_{K,\text{eff}} = 250$ mT. For all of these simulations, the magnetization state toggles from $m_z = -1$ to $m_z = +1$ state and thus confirms the robustness of this switching mechanism to thermal noise.

provides a larger toggle range ratio for fast rise times; however, as the rise time increases, the larger toggle range ratios can be achieved with smaller anisotropy. Furthermore, this toggle switching is robust to thermal

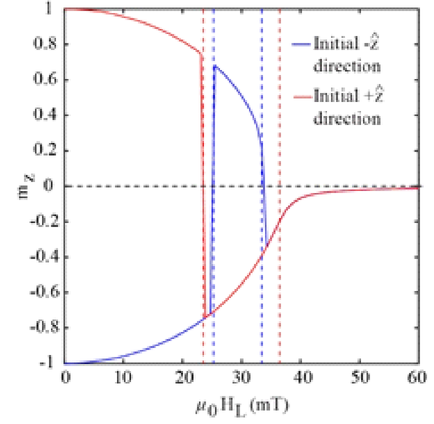

FIGURE 9. Analysis of fixed ferromagnet coupling impact on toggle switching for 1 mT dipolar field acting on the free ferromagnet in $-\hat{z}$-direction. The vertical red and blue dashed lines represent the toggle range for initial magnetization antiparallel and parallel to the fixed ferromagnet direction, respectively. The $\mu_0 H_L$ range bounded by the blue lines is shared by both toggle directions, and therefore determines the effective toggle range. The presence of dipolar fields thus decreases the toggle range when the initial free layer magnetization is parallel to the dipolar field, and increases it when the initial free layer magnetization is antiparallel to the dipolar field. For the parameters evaluated in these simulations, there is no toggle switching if the dipolar field is greater than ∼2.5 mT. This issue can be resolved with the dipolar field from a compensating ferromagnet.

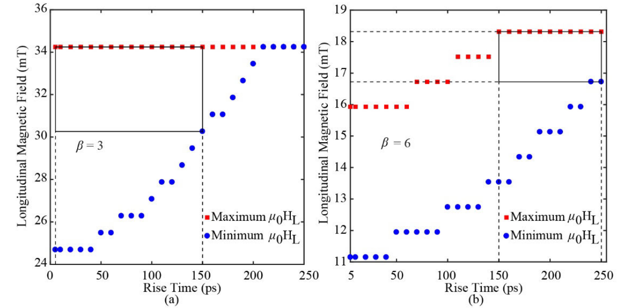

FIGURE 10. Rise time versus SOT field for the toggle operation for (a) $\beta = 3$ and (b) $\beta = 6$. For (a), where only a half precession around the hard axis is possible, only the minimum SOT field is sensitive to rise time. However, for (b), where both half and full precessions are possible, both the minimum and maximum boundary lines are sensitive to rise time. Even though both the maximum and minimum $\mu_0 H_L$ increase with t_{rise}, the toggle range and toggle range ration is smaller for $\beta = 6$ as compared to $\beta = 3$. It should be noted, however, that the use of a higher β provides a larger input range for inputs with a long rise time. The boxes in the figures show promising ranges of proper toggle switching, which can be used as specifications for the driver circuit.

effects, as demonstrated by the room temperature simulations of Fig. 8. These room temperature simulations also validate the suggested SOT excited stable state threshold of $m_z = |0.2|$.

To facilitate the design of these toggle SOT MRAM devices and circuits, the effects of dipolar coupling fields

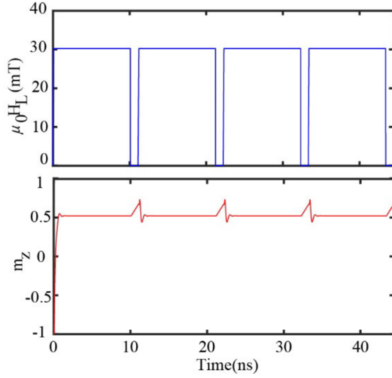

FIGURE 11. When insufficient relaxation time is provided, the toggle switching does not occur. In this case, the SOT pulses are only separated by 1 ns, which is not long enough to relax $\hat{m}$ vertically. As a result, the angular difference between $\hat{m}$ and $\hat{\sigma}$ after the 1 ns relaxation period is insufficient for precessional torque to cause $\hat{m}$ to cross the hard *x-y* plane.

have been explored and guidelines have been provided for selecting the SOT current magnitude and timing. As shown in Fig. 9, the presence of a coupling field from the fixed ferromagnet can cause asymmetric switching behavior, where the toggle range is broader for the magnetization favored by the fixed ferromagnet. Given the expectation of imprecision in the magnitude and rise time of the applied SOT current pulse, Fig. 10 depicts an approach to select nominal SOT pulse characteristics that maximize the robustness of the switching. As shown in the figure, bounding boxes are found with maximum height and width; the ideal nominal SOT current pulse magnitude and rise time are found near the center of these bounding boxes. Finally, Fig. 11 illustrates the importance of providing sufficient time for relaxation; if two SOT current pulses are provided within too small a time period, the MRAM will not relax sufficiently following the first SOT pulse to enable toggling by the second SOT pulse.

IV. CONCLUSION

In conclusion, toggle switching is a simple and effective approach for SOT-MRAM with PMA, and provides increased robustness than directional switching. The use of toggle switching and the increased robustness both reduce the hardware overhead of the write circuits, and the simplified device structure further reduces the area and improves the energy efficiency of MRAM caches. This proposed toggle MRAM device therefore leverages the previously demonstrated toggle SOT-PMA switching to provide a promising pathway for the incorporation of PMA devices in a new generation of compact, highly-efficient, and robust MRAM with SOT switching.

APPENDIX

The Landau–Lifshitz–Gilbert (LLG) equation describes magnetization dynamics in ferromagnetic materials

$$\frac{\partial \hat{m}}{\partial t} = -\gamma \hat{m} \times \vec{B}_{\text{net}} + \alpha \hat{m} \times \frac{\partial \hat{m}}{\partial t} \tag{3}$$

where $\hat{m}$ is a unit vector representing the normalized magnetization of the free ferromagnet, γ is the gyromagnetic ratio, α is the Gilbert damping parameter, and t is time. The PMA and SOT terms are components of the net magnetic field, $\vec{B}_{\text{net}}$:

$$\vec{B}_{\text{PMA}} = \mu_0 H_{K,\text{eff}}(\hat{m} \cdot \hat{z})\hat{z} \tag{4}$$

$$\vec{B}_{\text{SOT}} = \mu_0 \left(H_L \left(\hat{m} \times \hat{\sigma}\right) + H_T \hat{\sigma}\right) \tag{5}$$

where $\mu_0 H_{K,\text{eff}}$ is the peak magnitude of the effective PMA magnetic field, $\hat{z}$ represents the unit vector along the easy axis direction, and $\hat{\sigma}$ is spin polarization direction of SOT current. H_L and H_T represent the damping- and field-like components of SOT, respectively, while the ratio between H_T and H_L is expressed as the field-to-damping component ratio, β. In this work, the H_L and H_T values are determined from the definition of the spin-Hall effect

$$H_L = \frac{J_{\text{SOT}} \hbar \theta_{\text{sh}}}{2e\mu_0 M_s t_{\text{FM}}} \tag{6}$$

and

$$H_T = \beta H_L \tag{7}$$

where J_{SOT} is the in-plane current density that is injected through the heavy metal layer, θ_{sh} is the effective spin Hall angle, M_S is the saturation magnetization in A/m, and t_{FM} is the free ferromagnet thickness. It is important to note that $\mu_0 H_L \left(\hat{m} \times \hat{\sigma}\right)$ and $\mu_0 H_T \hat{\sigma}$ are sometimes referred to as the longitudinal and transverse magnetic fields, respectively [22].

Simulations were performed using mumax3 [18], an open-source GPU-accelerated micromagnetic simulation software that integrates the LLG equation of motion with a Finite Difference approach.

The magnetic parameters for the circular monodomain free ferromagnet are taken from Zhang *et al.* [19] which include: saturation magnetization $\mu_0 M_s = 1.3$ T, effective anisotropy field $\mu_0 H_{K,\text{eff}} = 250$ mT, Gilbert damping factor $\alpha = 0.02$, field to damping component ratio $\beta = 2$, as well as the following dimensions: FM layer diameter $D = 30$ nm, thickness $= 1.2$ nm. The discretization cell size for the simulation is taken to be 1.875 nm × 1.875 nm × 1.2 nm.

ACKNOWLEDGMENT

The authors would like to thank E. Laws, J. McConnell, N. Nazir, and L. Philoon for technical support.

REFERENCES

[1] S. Tehrani, J. M. Slaughter, E. Chen, M. Durlam, J. Shi, and M. DeHerren, "Progress and outlook for MRAM technology," *IEEE Trans. Magn.*, vol. 35, no. 5, pp. 2814–2819, Sep. 1999.

[2] S. Tehrani, "Status and outlook of MRAM memory technology (invited)," in *IEDM Tech. Dig.*, Dec. 2006, pp. 1–4.

[3] S. P. Park, S. Gupta, N. Mojumder, A. Raghunathan, and K. Roy, "Future cache design using STT MRAMs for improved energy efficiency: Devices, circuits and architecture," in *Proc. 49th Annu. Design Autom. Conf. (DAC)*, 2012, pp. 492–497.

[4] L. You *et al.*, "Switching of perpendicularly polarized nanomagnets with spin orbit torque without an external magnetic field by engineering a tilted anisotropy," *Proc. Nat. Acad. Sci. USA*, vol. 112, no. 33, pp. 10310–10315, Aug. 2015.

[5] M. Cubukcu *et al.*, "Spin-orbit torque magnetization switching of a three-terminal perpendicular magnetic tunnel junction," *Appl. Phys. Lett.*, vol. 104, no. 4, Jan. 2014, Art. no. 042406.
[6] M. Cubukcu *et al.*, "Ultra-fast perpendicular spin–orbit torque MRAM," *IEEE Trans. Magn.*, vol. 54, no. 4, Apr. 2018, Art. no. 9300204.
[7] G. Yu *et al.*, "Switching of perpendicular magnetization by spin–orbit torques in the absence of external magnetic fields," *Nature Nanotechnol.*, vol. 9, no. 7, pp. 548–554, Jul. 2014.
[8] M. Akyol *et al.*, "Current-induced spin-orbit torque switching of perpendicularly magnetized Hf|CoFeB|MgO and Hf|CoFeB|TaO_x structures," *Appl. Phys. Lett.*, vol. 106, no. 16, 2015, Art. no. 162409.
[9] S. Fukami, C. Zhang, S. DuttaGupta, A. Kurenkov, and H. Ohno, "Magnetization switching by spin-orbit torque in an antiferromagnet-ferromagnet bilayer system," *Nature Mater.*, vol. 15, no. 5, pp. 535–541, Feb. 2016.
[10] Q. Ma, Y. Li, D. B. Gopman, Y. P. Kabanov, R. D. Shull, and C. L. Chien, "Switching a perpendicular ferromagnetic layer by competing spin currents," *Phys. Rev. Lett.*, vol. 120, no. 11, Mar. 2018, Art. no. 117703.
[11] Z. Wang, Z. Li, M. Wang, B. Wu, D. Zhu, and W. Zhao, "Field-free spin–orbit-torque switching of perpendicular magnetization aided by uniaxial shape anisotropy," *Nanotechnology*, vol. 30, no. 37, Sep. 2019, Art. no. 375202.
[12] J. M. Lee *et al.*, "Field-free spin–orbit torque switching from geometrical domain-wall pinning," *Nano Lett.*, vol. 18, no. 8, pp. 4669–4674, Aug. 2018.
[13] W. Legrand, R. Ramaswamy, R. Mishra, and H. Yang, "Coherent subnanosecond switching of perpendicular magnetization by the fieldlike spin-orbit torque without an external magnetic field," *Phys. Rev. Appl.*, vol. 3, no. 6, Jun. 2015, Art. no. 064012.
[14] B. N. Engel *et al.*, "A 4-Mb toggle MRAM based on a novel bit and switching method," *IEEE Trans. Magn.*, vol. 41, no. 1, pp. 132–136, Jan. 2005.
[15] Z. Wang *et al.*, "Evaluation of ultrahigh-speed magnetic memories using field-free spin–orbit torque," *IEEE Trans. Magn.*, vol. 54, no. 11, Nov. 2018, Art. no. 3401505.
[16] D. Apalkov, B. Dieny, and J. M. Slaughter, "Magnetoresistive random access memory," *Proc. IEEE*, vol. 104, no. 10, pp. 1796–1830, Oct. 2016.
[17] M. Yamanouchi *et al.*, "Three terminal magnetic tunnel junction utilizing the spin Hall effect of iridium-doped copper," *Appl. Phys. Lett.*, vol. 102, no. 21, May 2013, Art. no. 212408.
[18] A. Vansteenkiste, J. Leliaert, M. Dvornik, M. Helsen, F. Garcia-Sanchez, and B. Van Waeyenberge, "The design and verification of MuMax3," *AIP Adv.*, vol. 4, no. 10, Oct. 2014, Art. no. 107133.
[19] C. Zhang, S. Fukami, H. Sato, F. Matsukura, and H. Ohno, "Spin-orbit torque induced magnetization switching in nano-scale Ta/CoFeB/MgO," *Appl. Phys. Lett.*, vol. 107, no. 1, Jul. 2015, Art. no. 012401.
[20] J. Torrejon *et al.*, "Current-driven asymmetric magnetization switching in perpendicularly magnetized CoFeB/MgO heterostructures," *Phys. Rev. B, Condens. Matter*, vol. 91, no. 21, Jun. 2015, Art. no. 214434.
[21] Y. Chen, H. Celik, T. Wang, H. Kannan, I. N. Krivorotov, and J. Q. Xiao, "Quantifying angular dependence of spin-orbit torques in Ta/CoFeB/MgO trilayers with perpendicular magnetic anisotropy," *Phys. Rev. B, Condens. Matter*, vol. 95, no. 14, Apr. 2017, Art. no. 144405.
[22] C. Zhang *et al.*, "Magnetotransport measurements of current induced effective fields in Ta/CoFeB/MgO," *Appl. Phys. Lett.*, vol. 103, no. 26, Dec. 2013, Art. no. 262407.

NAIMUL HASSAN (S'18) received the B.Sc. degree in electrical and electronic engineering from the Bangladesh University of Engineering and Technology, Dhaka, Bangladesh, in 2016. He is currently pursuing the Ph.D. degree in electrical engineering with the Erik Jonsson School of Engineering and Computer Science, The University of Texas at Dallas, Richardson, TX, USA.

His current research focuses on spintronic memory and neuromorphic devices.

SUSANA P. LAINEZ-GARCIA is currently pursuing the B.S. degree in electrical engineering with the Erik Jonsson School of Engineering and Computer Science, The University of Texas at Dallas, Richardson, TX, USA.

Her current research focuses on spintronic memory and neuromorphic devices.

FELIPE GARCIA-SANCHEZ (S'04–M'08) received the B.S. degree in physics from the Universidad de Zaragoza, Zaragoza, Spain, and the Ph.D. degree in physics from the Universidad Autonoma de Madrid, Madrid, Spain, in 1998 and 2007, respectively.

He has worked for various scientific institutions in France, Germany, and Italy. He currently works as a Postdoctoral Researcher with the Universidad de Salamanca, Salamanca, Spain, to study the magnetization switching by optical manipulation. He has published 53 papers in the area of physics. His current research interests include spintronic devices and magnetization dynamics.

JOSEPH S. FRIEDMAN (S'09–M'14–SM'19) received the A.B. and B.E. degrees from Dartmouth College, Hanover, NH, USA, in 2009, and the M.S. and Ph.D. degrees in electrical and computer engineering from Northwestern University, Evanston, IL, USA, in 2010 and 2014, respectively.

He joined The University of Texas at Dallas, Richardson, TX, USA, in 2016, where he is currently an Assistant Professor of electrical and computer engineering and the Director of the NeuroSpinCompute Laboratory. From 2014 to 2016, he was a Centre National de la Recherche Scientifique Research Associate with the Institut d'Electronique Fondamentale, Université Paris-Sud, Orsay, France. He has also been a Summer Faculty Fellow with the U.S. Air Force Research Laboratory, Rome, NY, USA, a Visiting Professor with the Politecnico di Torino, Turin, Italy, a Guest Scientist with RWTH Aachen University, Aachen, Germany, and worked on logic design automation as an intern with Intel Corporation, Santa Clara, CA, USA.

Dr. Friedman is a member of the editorial board of *Microelectronics Journal*, the technical program committees of DAC, DATE, SPIE Spintronics, NANOARCH, GLSVSI, and ICECS, the review committee of ISCAS, and the IEEE Circuits and Systems Society Nanoelectronics and Gigascale Systems Technical Committee. He has been a member of the organizing committee of NANOARCH 2019 and DCAS 2018. He has also been awarded a Fulbright Postdoctoral Fellowship. His research interests include the invention and design of novel logical and neuromorphic computing paradigms based on nanoscale and quantum mechanical phenomena, with particular emphasis on spintronics.